ACS APPLIED MATERIALS & INTERFACES

Research Article

www.acsami.org

Surface Engineered CuO Nanowires with ZnO Islands for CO_2 Photoreduction

Wei-Ning Wang,[†] Fei Wu,[‡] Yoon Myung,[‡] Dariusz M. Niedzwiedzki,[§] Hyung Soon Im,[∥] Jeunghee Park,[∥] Parag Banerjee,*[,‡] and Pratim Biswas*[,†]

[†]Aerosol and Air Quality Research Laboratory, Department of Energy, Environmental and Chemical Engineering, Washington University in St. Louis, St. Louis, Missouri 63130, United States

[‡]Laboratory for Emerging and Applied Nanomaterials, Mechanical Engineering & Materials Science, Washington University in St. Louis, St. Louis, Missouri 63130, United States

[§]Photosynthetic Antenna Research Center (PARC), Washington University in St. Louis, St. Louis, Missouri 63130, United States

[∥]Department of Chemistry, Korea University, Jochiwon 339-700, Korea

Supporting Information

ABSTRACT: Large arrays of massively parallel (10^8 cm^{-2}) CuO nanowires were surface engineered with dense ZnO islands using a few pulsed cycles of atomic layer deposition (ALD). These nanowires were subjected to UV−vis radiation-based CO_2 photoreduction under saturated humidity (CO_2 + H_2O mixture) conditions. We monitored CO_2 to CO conversion, indicating the viability of these nanostructures as potential photocatalysts. High-resolution transmission electron microscopy and atomic force microscopy indicated an island growth mechanism of ZnO epitaxially depositing on pristine, single crystal CuO nanowire surface. Photoluminescence and transient absorption spectroscopy showed a very high density of defects on these ZnO islands which trapped electrons and enhanced their lifetimes. Peak CO conversion (1.98 mmol/g-cat/hr) and quantum efficiency (0.0035%) were observed in our setup when the ZnO islands impinged each other at 1.4 nm (8 cycles of ALD) diameter; at which point ZnO island perimeter lengths maximized as well. A mechanism whereby simultaneous H_2O oxidation and CO_2 reduction occurred in the active perimeter region between CuO nanowire and ZnO islands is proposed to explain the observed photoconversion of CO_2 to CO.

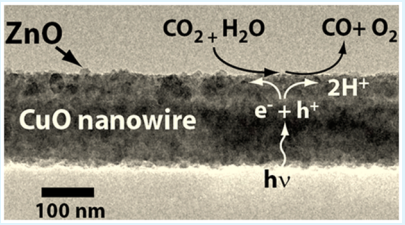

KEYWORDS: *CuO nanowires, ZnO, atomic layer deposition (ALD), CO_2 photoreduction, photoluminescence, time-resolved transient absorption spectroscopy*

INTRODUCTION

With global CO_2 levels reaching 400 ppm,[1,2] there is an urgency to develop impactful solutions for CO_2 remediation. An effective approach to counter CO_2 emissions is to convert it to value-added products, such as hydrocarbon fuels, which not only mitigates CO_2 emissions but also recycles it as a fuel feedstock.[3] It is desirable that inexpensive and benign coreactants (e.g., water) be used with abundant energy sources such as solar energy to photocatalyze and convert CO_2 into useful chemicals, the so-called CO_2 photoreduction process.[4−10] CO_2 photoreduction in engineered systems, however, still suffers from low conversion yields and quantum efficiencies, resulting from fast electron−hole recombination, narrow light absorption range, and backward reactions.[5,6,11,12] Strategies to improve yield have been a prominent quest.

Since Honda's pioneering work on TiO_2 photocatalysts,[4,13] solar photochemistry with research on new semiconducting nanomaterials is being recognized[14,15] as the pathway toward CO_2 remediation. To this effect, TiO_2 is still a popular photocatalyst for CO_2 photoreduction due to its favorable band edges. A disadvantage of using TiO_2 is its band gap (3.3 eV) which requires UV light to excite electrons from the valence band to the conduction band. Conversion yields of <250 μmol/g-cat/hr are routinely obtained.[5−10,16] Modifications to TiO_2 to enhance CO_2 photoreduction performance, such as doping/depositing metals,[17−19] making mesoporous matrix,[20−23] developing high aspect ratio nanostructures,[19,24] and incorporating photosensitive enzymes or dyes[16,25] have been tried. However, the above processes either use expensive metal catalysts with stability issues[26] or have scalability or capacity limits. Thus, there is a strong desire to develop new materials which can perform better than available TiO_2 based approaches, leading to the next generation of CO_2 photocatalyst materials.

Here, we report on the development of atomic layer deposition (ALD) ZnO coated CuO nanowires for the photocatalytic conversion of CO_2 to CO. Single crystalline, high-density (10^8 cm^{-2}) CuO nanowires were made by thermal oxidation of high purity copper (Cu) foils and ZnO was deposited by ALD (see experimental details in Materials and

Received: October 8, 2014
Accepted: February 27, 2015
Published: February 27, 2015

DOI: 10.1021/am508590j
ACS Appl. Mater. Interfaces 2015, 7, 5685−5692

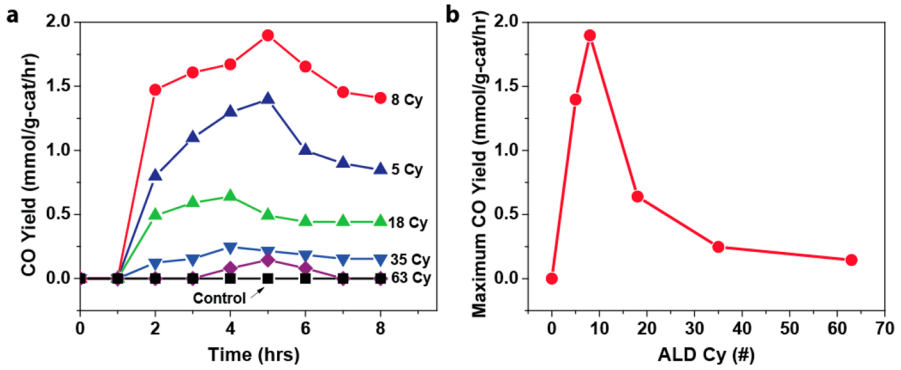

Figure 1. CO_2 photoreduction results. (a) CO yields of ZnO−CuO nanowires with different ZnO ALD cycles as a function of irradiation time. Results of control experiments were included as black squares. (b) Maximum CO yield as a function of ZnO ALD cycles.

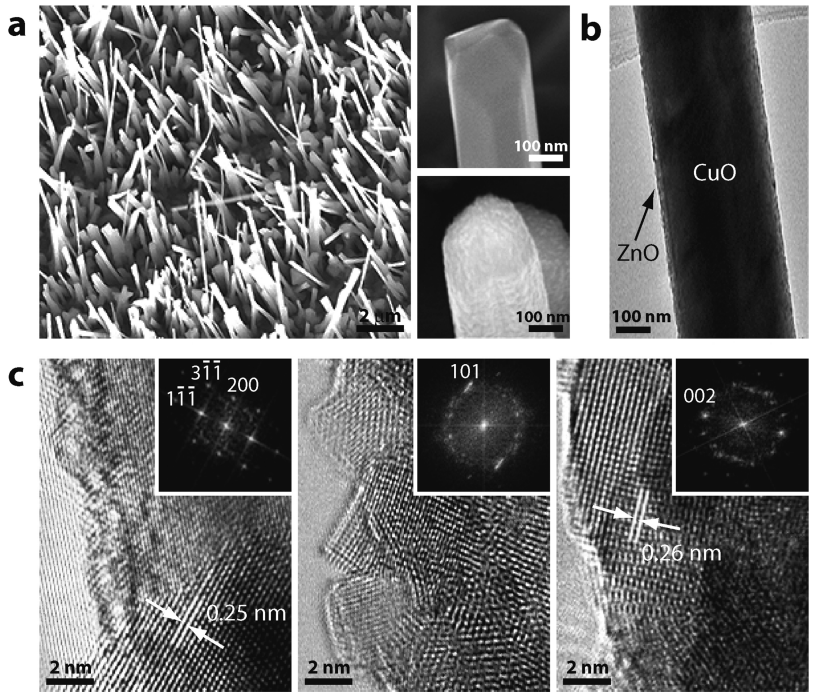

Figure 2. Characterization of representative CuO and ZnO−CuO nanowires. (a) FE-SEM image of ZnO−CuO nanowire arrays with magnified pristine CuO nanowire (upper right) and 63 cycles of ALD ZnO coated CuO nanowire (lower right). (b) TEM image of 63 cycles of ALD ZnO coated single CuO nanowire. (c) HRTEM and corresponding FFT electron diffraction patterns of pure single crystalline CuO (left), 5 cycles of ALD ZnO coated (middle), and 63 cycles of ALD ZnO coated CuO nanowire surface (right).

Methods). Several unique aspects of this work are (1) the new composite material does not use noble metal catalyst nanoparticles which are commonly used in other CO_2 photoreduction schemes; (2) the raw materials are abundant, and CuO with a bandgap of 1.53 eV is better matched to the solar spectrum than pristine ZnO; (3) interfacing *p*-type CuO with *n*-type ZnO leads to suitable alignment of band edges that favor electron−hole separation; and (4) processes for making the material are highly scalable. The importance of controlling surface morphology and surface composition of the photocatalyst is highlighted; this is also utilized to unravel the mechanistic aspects of photoreduction on these atomically engineered surfaces.

RESULTS AND DISCUSSION

Carbon Dioxide Photoreduction using ZnO−CuO Composite Nanowires. The ZnO−CuO nanowires with different ZnO ALD cycles were subjected to CO_2 photoreduction (see Materials and Methods and Supporting Information, S2).[19] CO was the major product based on the two electron photoreduction reaction:[4,19]

$$CO_2 + 2H^+ + 2e^- \rightarrow CO + H_2O \quad (1)$$

From an application perspective, while direct conversion to a hydrocarbon fuel, such as methane may be preferred, reducing CO_2 to syngas (CO and H_2) is also desirable, as the chemical industry is well set up to produce a range of downstream products from syngas.[27] Hydrogen (H_2) evolution was not observed, indicating that the consumption of protons and electrons based on the following reaction ($2H^+ + 2e^- \rightarrow H_2$) is not significant, which in turn favors the formation of CO. This reaction requires the simultaneous photooxidation of H_2O and production of protons given as:

$$H_2O + 2h^+ \rightarrow \frac{1}{2}O_2 + 2H^+ \quad (2)$$

DOI: 10.1021/am508590j
ACS Appl. Mater. Interfaces 2015, 7, 5685−5692

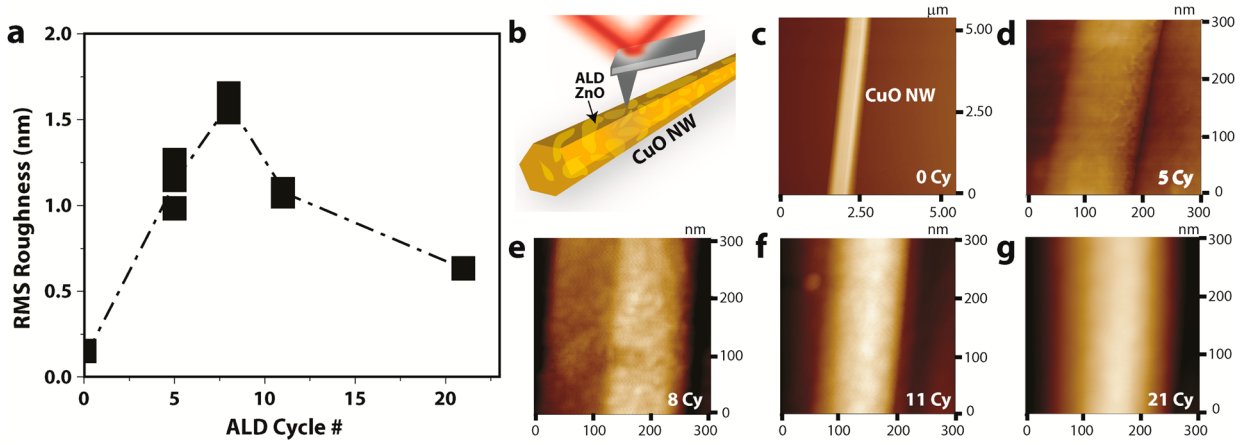

Figure 3. Surface roughness characterization by AFM. (a) RMS roughness as a function of ALD ZnO cycles. (b) Schematic of AFM measurements on ZnO islands on CuO nanowires. (c–g) Series of AFM images showing the surface roughness on single CuO nanowire as the number of ALD ZnO cycles increase from 0 to 21 cycles. Scan size and height are adjusted to best capture the texture of the growing film on a single facet of the wire. Roughness was measured locally and at multiple locations of equal area on the surface of the CuO nanowires.

From Figure 1a, the ZnO–CuO nanowires demonstrated a maximum CO yield achieved was 1.98 mmol/g-cat/hr for the 8 ALD cycle sample. This yield is specific to the experimental set up used in this work. The mass of the exposed CuO nanowires was used to estimate the net conversion yields (Supporting Information, S1). The quantum yield at this condition was calculated to be 0.0035% (Supporting Information, S4), which is low but not unusual for CO_2 photoreduction reactions.[28] After 5 h of irradiation, the CO yield started to decline slightly, because of diminishment of the adsorption power of the catalyst and the saturation of adsorption sites on the catalyst surface with intermediate products.[12,19] Similar to our previous report,[19] the volumetric ratio of O_2/N_2 (not shown), another important indicator for proton generation based on eq 2, reveals a similar tendency as that of CO formation. A time dependency on the CO yield was also observed, which can be attributed to the adsorption/reaction/desorption of gases on the catalyst surface. Assuming Langmuir adsorption-based kinetics, an exponential saturation curve was used to model this behavior, that is, CO Yield = $A[1-\exp(-t/\theta)]$, where A is constant, t is time, and θ is the kinetic parameter that quantifies the rate of CO yield. It was found that θ varied as 80, 36, 42, and 240 min for 5, 8, 18, and 35 cycles of ZnO, respectively. The fastest reaction rate (smallest θ) was found for the 8 cycle sample.

Further, we report on control experiments (Figure 1a). The first control experiment was performed using pristine CuO nanowires. No CO_2 photoreduction was observed. Utilizing bare ZnO layer (thickness = 1.4 nm) deposited on an indium tin oxide (ITO) substrate did not yield any CO either. Theoretically, ZnO is a good photocatalyst for CO_2 photoreduction. However, the ZnO layer may not be activated if the thickness is below the effective absorption depth. Finally, CO_2 was replaced with N_2 gas to rule out the possibility of surface carbon contamination. No carbon-based products were detected indicating that these nanowires have negligible adventitious carbon. Thus, any CO detected from the following CO_2 photoreduction analyses would come from CO_2 gas.

From the above discussion, it is clear that neither pure CuO nanowires nor ultrathin ZnO layer by itself was responsible for CO_2 photoreduction. However, a combination of ZnO on CuO nanowires led to effective CO production. Based on reactions given by eqs 1 and 2, both ZnO and CuO surfaces determine the photoreduction yield of CO_2.

The ZnO thickness, represented by the number of ALD cycles, plays an important role in CO_2 photoreduction (Figure 1b). The CO yield first increases with increasing ALD cycles with the optimal thickness at 8 cycles. Beyond the optimal condition, the ZnO–CuO nanowires demonstrate lower CO yields. These results indicate that ZnO thickness also is critical in determining catalyst yield.

Interface and Structural Analyses using Electron Microscopy. Detailed structural and morphological analyses by field emission scanning electron microscopy (FE-SEM) and transmission electron microscopy (TEM) were performed on pristine CuO and ZnO–CuO nanowires (Figure 2). High density CuO nanowire arrays are observed in Figure 2a. The average diameter and length of the nanowires are about 230 nm and 1.2 μm, respectively, which can be tuned by changing temperature, time, and oxygen concentration.[29] The surface of the pristine CuO nanowire is faceted and fairly smooth (upper right, Figure 2a), indicating that these nanowires have high crystallinity.[30] In comparison, after 63 cycles of ZnO, the surface of CuO nanowires became rough with ZnO grains (lower right, Figure 2a). A representative TEM image of a 63 cycle nanowire is shown in Figure 2b, where a continuous and crystalline ZnO film is observed.

To investigate the surface structure of the nanowires, we also performed high-resolution (HR) TEM analysis. HRTEM images are shown in Figure 2c with corresponding fast Fourier transfer (FFT) electron diffraction patterns. It is apparent that the pristine CuO nanowire mainly consists of $(\bar{1}11)$ plane (interplanar spacing = 0.252 nm), which was reported by other groups as well (Figure 2c, left).[30] For 5 cycle sample (Figure 2c, middle), discrete and well-defined ZnO crystals are seen on the CuO surface. This is surprising because ALD is known for being a conformal, layer-by-layer deposition process. However, under substrate-inhibited growth conditions (such as pristine single crystal surfaces with little or no surface defects), a nucleation and growth mechanism may be active and result in an "incubation" period for the ALD film before continuous layer-by-layer growth occurs.[31−33] As indicated in its FFT pattern, the major ZnO plane is (101) with the lattice distance of 0.248 nm, matching closely with the CuO $(\bar{1}11)$ plane. This

DOI: 10.1021/am508590j
ACS Appl. Mater. Interfaces 2015, 7, 5685−5692

indicates that the initial growth of ZnO is determined by the crystallography of underlying CuO nanowires following the epitaxial relationship, CuO ($\bar{1}11$) || ZnO (101).[34,35] It is to be noted that the ZnO (101) plane is a polar, low symmetry plane.[31−33]

After the 63-cycle sample (Figure 2c, right), the primary ZnO plane changed from (101) to (002) plane with a smoother surface. The possible pathway for this structural and crystallographic transformation can be understood by considering a nucleation and growth mechanism for ALD ZnO thin films. While the epitaxial matching between CuO and ZnO determines initial nucleation of the discrete pyramidal-like nanocrystals with ZnO (101) exposed surface, continuous growth leads to the merging of these surfaces and the formation of a crystalline ZnO film with *c* axis orientation. It is to be noted that the (002) plane is polar in nature (either O- or Zn-terminated).[31]

Morphological Evolution of ZnO Film on CuO Nanowire Surface. Next, atomic force microscopy (AFM) analysis of the ZnO−CuO nanowires during the initial ALD cycles was carried out. As shown in Figure 3a, the root-mean-square (RMS) surface roughness of the nanowires increases initially until eight cycles. Past eight cycles, the roughness starts to decrease. This behavior suggests a nucleation and growth mechanism for thin film growth. During the nucleation phase, discrete islands contribute to surface roughness. Once the islands impinge neighboring nuclei, islands merge to form a conformal film. The size of the ZnO islands is determined by the ALD cycles where, eight cycles correspond to a thickness of 1.4 nm (deposition rate = 0.17 nm on Si[36]). The RMS roughness trend observed in Figure 3a matches the CO_2 photoreduction data in Figure 1b. The striking resemblence between CO_2 photoreduction response with ALD cycles and surface roughness variation of ZnO, reiterates the fact that surface morphology plays a critical role in determining high CO_2 photoreduction yields.

The morphology of the nanowire facets with changing ALD cycles (0, 5, 8, 11, and 21 cycles) are shown in Figure 3c−g, where the surface textures of these nanowires are visible. For instance, a smooth surface is observed for pristine CuO nanowires in Figure 3c. But for ZnO−CuO nanowires, in particular for 5 and 8 cycles, discrete ZnO islands can be identified. The results are consistent with our FESEM and TEM analyses (Figure 2).

Photoluminescence and Defect Studies. To understand CO_2 photoreduction pathways, photoluminescence (PL) measurements of pristine CuO and ZnO−CuO nanowires were conducted (Figure 4; Supporting Information, S5 and Table S1). CuO nanowires show a broad emission peak from 400 nm −700 nm, similar to the recent reports. Othonos et al.[37] showed broad PL spectra much closer to the one observed in this work and assign the peaks to recombination of intra valence band (VB) electrons with simultaneous contributions from midgap defect states.

The ZnO−CuO nanowires exhibit a typical ZnO PL spectra with a relatively sharp UV band and a broad visible emission band, attributed to excitonic recombination (near band emission, NBE = 381 nm) and recombination related to structural and surface defects,[38−40] respectively.

For the 5-cycle sample, where discrete ZnO nanocrystals are observed, the defect-related green emission dominates the PL response. The ratio of intensity of NBE to defect peaks, I_{NBE}/I_{defect}, was 0.25 indicating surface defects determine much of the

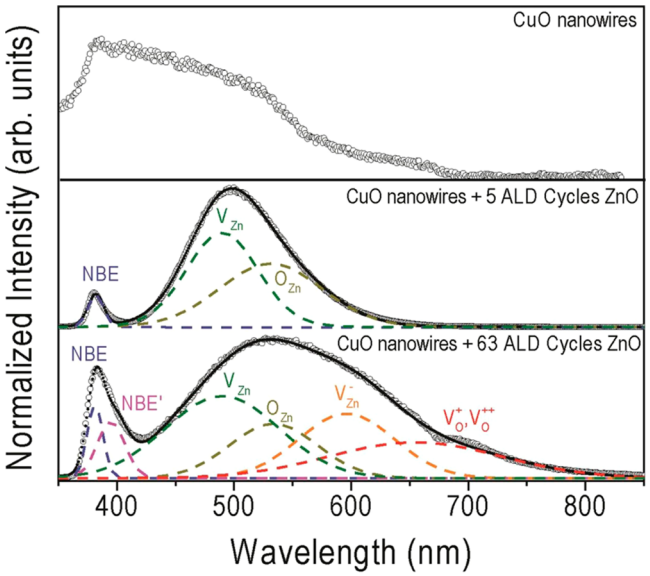

Figure 4. Room temperature photoluminescence spectra of CuO and ZnO−CuO nanowires. CuO nanowires (top) show a broad emission between 400 and 700 nm related to valence intraband transitions. For 5 ALD cycles ZnO−CuO nanowires (middle), a near band emission (NBE) is seen while a strong defect related emission is observed, which can be deconvoluted to belong to V_{Zn} and O_{Zn} defects, both residing close to the VB edge. For 63-cycle ZnO−CuO sample, (bottom) a stronger NBE and NBE′ is observed. The defect-related emission consists of four distinct peaks associated with defects lying close to the VB (V_{Zn}, O_{Zn}) and CB edges (V_{Zn}^{-}, V_O^{+}, V_O^{+2}).

electronic and optical properties.[41] Further, two peaks can be deconvoluted from the defect band emission: acceptor-like vacancy of zinc (V_{Zn}, 489 nm) and antisite oxygen (O_{Zn}, 531 nm).[42] The green emission has been linked to Cu^{2+} impurities (433 nm) given the proximity to the CuO surface.[43] However, our PL data does not suggest any Cu^{2+}-related peaks.

For the 63-cycle sample, I_{NBE}/I_{defect} was 0.78, indicating reduced impact of the surface states as compared to the 5-cycle sample. The film crystallinity is better developed, and defects, while present, have a lower PL intensity.[41] The UV band can be deconvoluted into two separate peaks—NBE and NBE′ (395 nm). While NBE belongs to single crystalline ZnO, NBE′ is due to internal stresses in the film.[44] These stresses can be formed due to coalescence of nanocrystals as these impinge on one another. The NBE peak detected in this work is much sharper, indicating better crystallinity than those reported previously.[45] This is possibly due to better epitaxial matching of the ZnO (101) deposited with the underlying CuO ($\bar{1}11$) nanowires. Two additional defect-related peaks, donor-like, monovalent vacancies of zinc (V_{Zn}^{-}) and single- and double-ionized oxygen vacancies (V_O^{+} and V_O^{2+})[39] are also observed.

Transient Absorption Spectroscopy of CuO and ZnO−CuO Nanowires. Figure 5a shows representative transient absorption (TA) spectra of CuO nanowires taken at various delay times after excitation at 325 nm. It is known that trapping photoexcited electrons in the conduction band (CB) occurs on time scales of 100−200 fs,[46] which is close to the temporal resolution of the spectrometer, and this process cannot be sufficiently resolved. The early TA spectra (0.7 ps) contain characteristic negative bands at ∼490 and 610 nm, similar to the bands present in the PL spectra of CuO nanowires (Figure 4). When the scaled (factor = 0.4) 0.7 ps TA spectrum is

DOI: 10.1021/am508590j
ACS Appl. Mater. Interfaces 2015, 7, 5685−5692

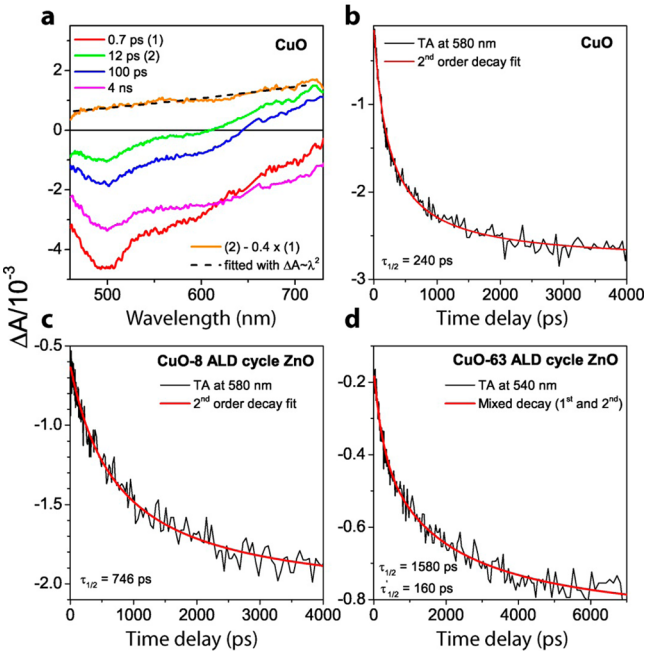

Figure 5. Transient absorption results of CuO and ZnO−CuO nanowires. (a) Representative TA spectra of CuO nanowires taken at various delay times. The orange line corresponds to the predicted TA spectrum of shallowly trapped electrons promoted to CB after laser photoexcitation. The spectrum was fitted with theoretical function with parameters provided in the figure; (b−d), demonstrative kinetic traces extracted from TA data sets of each sample accompanied by fits. The dynamic parts of kinetic traces are associated with recombination of electron−hole pairs and can be successfully fitted with a second-order decay, except for panel d, which was fitted by both first and second order decays.

subtracted from the 12 ps TA spectrum, an elevated positive transient signal spanning the entire spectral range is obtained, indicating the presence of photoexcited, shallowly trapped electrons in the CB. Theoretically, absorption of such "free" electrons is proportional to the square of absorbing wavelength and such simulative fit is also provided (dashed line, Figure 5a).[47]

Upon the assumption that bleaching of absorption bands is practically constant within the range of spectrometer time window, the dynamic properties of recombination of weakly trapped electrons with holes may be obtained from the direct fitting of kinetic traces probed at wavelengths in which TA of these electrons occurs. Figure 5b−d shows representative TA dynamics of the CuO and ZnO−CuO nanowires. The fitting details are provided in Supporting Information, S3.[48] TA data suggest that electrons, once transferred from the CB of CuO nanowires to ZnO islands, should experience at least 3 times longer recombination half-lifetime. This is in line with recently published results.[35]

Mechanism of CO_2 Photoreduction in ZnO−CuO Nanowires. Taken together, the results obtained suggest that the CO_2 photoreduction performance observed in ZnO−CuO nanowires result from three primary sources. First, the choice of material is important. The deposition of ZnO on CuO allows favorable band alignment of the CuO and ZnO conduction and VB edges (Figure 6). The bandgap of CuO (1.53 eV; Figure S3b, Supporting Information) is well suited for visible light absorption, and the band alignment provides suitable electron transfer from the CuO to ZnO and hole

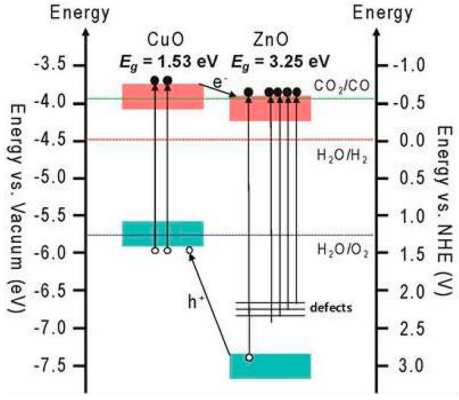

Figure 6. Band diagram of the CO_2 photoreduction process in ZnO−CuO nanowires. Band alignment of the nanowires and their energy levels with respect to vacuum (left y axis) and normal hydrogen electrode (NHE) (right y axis) are illustrated.

transfer from ZnO to CuO. Further, the CuO ($\bar{1}11$) plane allows epitaxial growth of the ZnO (101) and creates a defect free interface between the two disparate materials and allows for recombination free charge transfer.

Second, and more importantly, the surface morphology proves to be critical the photoreduction process. TA data indicates that both 8-cycle ($\tau_{1/2}$ = 746 ps) and 63-cycle ($\tau_{1/2}$ = 1580 ps) samples exhibit higher electron lifetimes as compared to pristine CuO nanowires ($\tau_{1/2}$ = 240 ps). This confirms the favorable transfer of electrons from CuO and its extended lifetime in ZnO. However, the TA data by itself fails to explain the thickness dependency of CO_2 yield (Figure 1b), because according to the $\tau_{1/2}$ values, thicker ZnO films should generate higher CO yields. This inconsistency can be explained by considering the discrete island-like morphology of the 8-cycle sample as explained below.

Because the $CO_2 \rightarrow CO$ is a two-electron process requiring the presence of both electrons and H^+, we propose that exposure of both ZnO (for eq 1) and CuO (for eq 2) surfaces to the gas ambient is important. This is achieved by ALD of ZnO on CuO nanowires for up to eight cycles. We suggest that reaction eqs 1 and 2 occur around the perimeter of the ZnO nanocrystals—triple phase boundaries (Figure S4a, Supporting Information), where a rich source of both electrons and H^+ are simultaneously available. Past eight cycles, the ZnO nanocrystals merge and thus, conformally cover all exposed CuO nanowire surface (Figure 3a and Figure S4b−e, Supporting Information). This significantly reduces the photoreduction performance (Figure 1b) because H_2O, which requires an exposed CuO surface, is unable to be protonated.

Third and finally, surface defects play the most important role in the development of new materials for high-yield CO_2 photoreduction. Simple geometric modeling of the nucleation and growth phenomena yields a curve (Figure S4f, Supporting Information) similar to Figure 1b for nuclei densities of 1.4×10^{13} cm^{-2} and the maximum perimeter value fitted for eight cycles, just before nuclei coalescence occurs. When compared to typical cation areal densities in metal oxides[49] ($\sim 10^{15}$ atoms cm^{-2}), this nuclei represents clusters that consists of a few hundred ZnO molecular units only and thus highlights the effect of extremely high surface to volume ratio nanocrystals on catalytic activity. Indeed, our PL data shows that such nanocrystals have a high concentration of surface defects. Low quantum yields (0.0035%) are therefore not surprising,

DOI: 10.1021/am508590j
ACS Appl. Mater. Interfaces 2015, 7, 5685−5692

given such high density of surface defects. Regardless, the ZnO surfaces lead to defect-mediated activated adsorption, reaction, and desorption of molecules and are reflected in the combined kinetics of the CO yield (derived from Figure 1a) that shows the eight-cycle sample with the fastest mean time to saturation of $\theta \sim 36$ min.

We finally note that structurally, the (101) plane of ZnO is a charged surface consisting of, on an average, two unterminated bonds associated for tetragonally coordinated Zn^{2+} or O^{2-} ions. On the other hand, the (002) plane is charged, too, but consists of one unterminated bond per ion. Theoretical investigations have shown that the (101) plane is more unstable than the (002) plane.[50] The presence of a high density of unterminated bonds and the inherent instability of the (101) surface, may lead to enhanced CO_2 adsorption and reaction on this surface. Thus, surface defects contribute to the enhancement of CO_2 photoreduction performance in the ZnO−CuO nanowire system.

CONCLUSIONS

In summary, we have discovered that a few nanometers of ZnO on CuO nanowires acts as photocatalyst for the conversion of CO_2 to CO. Our results indicate a yield of at least 1.98 mmol/g-cat/hr and a quantum efficiency of 0.0035% on the experimental setup used in this work. The materials combination of ZnO and CuO obviates the use of expensive and noble metal catalysts. The epitaxy observed between CuO nanowire and ZnO allows favorable and recombination-free electron transfer from the CuO nanowire to the ZnO. The island morphology of the ZnO naturally creates exposed regions of both CuO and ZnO surfaces on the nanowires. This island morphology can be controllably varied in crystalline orientation and texture by varying the cycle numbers of the ALD ZnO. Variation of CO_2 to CO yield with ALD ZnO cycle numbers strongly suggests that the availability of both CuO and ZnO surfaces is necessary for the oxidation and reduction half-reactions to occur during the photoreduction of CO_2. Yields maximize when the ZnO islands are just impinging on each other and island perimeter lengths maximize. The high concentration of surface defects on the (101) exposed ZnO islands lead to the trapping of the transferred electrons, long enough for the effective photoconversion of adsorbed CO_2 to CO. This work lays the groundwork and design rules for future surface nanoengineered, all-metal oxide, nanowire photocatalysts.

MATERIALS AND METHODS

Materials Synthesis. First, 127 μm thick Cu foils were purchased from VWR International with a purity of 99.9%. Then, the foils were cut into 1 × 1 cm pieces, and surface native oxide was removed by placing the pieces in 1 M HCl solution for 30 min. The foils were then immediately put into a tube furnace maintained at 500 °C for 30 min at ambient pressure after being cleaned with deionized (DI) water and dried with compressed air. Dense CuO nanowires were grown on the surface of the foil. ALD was used to deposit different thicknesses of ZnO on CuO nanowires at 150 °C with a background pressure of 50 mTorr. Diethyl zinc with a purity of 99.9% (SAFC Hitech) and DI water were used as precursors, using a precursor pulse time of 1.5 and 1.0 s, respectively. Mass determination of CuO nanowires was done by thermogravimetric analysis, as shown in the Supporting Information, S1.

Materials Characterization and CO_2 Photoreduction Analysis. Nanowire morphology was examined using FE-SEM (JEOL-7001LVF) operated at 15 kV. The inner structure of the nanowires was analyzed by TEM (JEM-2100F, JEOL) at 200 kV. The FFT patterns were generated from the HRTEM images using Digital Micrograph GMS 1.4 (Gatan, Inc.). The optical property of the CuO nanowires was measured by vis−NIR absorption spectroscopy from which the bandgap of the nanowires was estimated. The morphology and RMS surface roughness of the pristine CuO and ZnO−CuO nanowires was analyzed by AFM (Dimension 3000, Digital Instruments). An 8 nm radius Si tip (MikroMasch, HQ:NSC35) was used in tapping mode to obtain AFM height images on multiple facets of CuO nanowires. Using Z-height statistics is a reliable method to probe the surface morphology during nucleation and growth,[49] and therefore, we focus on the RMS roughness. We carried out the steady-state photoluminescence measurements of these nanowires at room temperature using a He−Cd laser (λ = 325 nm) as the excitation source with 1 nm resolution. The PL spectra are fitted by Voigt functions.

The photoreduction analysis system has been detailed in the Supporting Information, S2, and our previous papers.[19,22] Briefly, compressed CO_2 with a flow rate of 3 mL/min was used as the carbon source, which passed through a water bubbler to generate a mixture of CO_2 and water vapor. The gaseous mixture was then fed into a continuous flow reactor, where the nanowires were loaded. The nanowires were activated by a Xe lamp (Oriel 66021, Newport Co.) operated at 400 W with an accumulated intensity of 300 mW/cm^2 in the wavelength range of 250−810 nm (see light spectrum in Figure S2b, Supporting Information). The concentrations of effluent gases as a function of irradiation time were recorded automatically by gas chromatography (GC) through an automated gas valve, equipped with a PLOT capillary column (Supelco Carboxen-1010) and a thermal conductivity detector.

Time-resolved pump−probe absorption experiments were carried out using Helios, a femtosecond TA spectrometer from Ultrafast Systems. Experimental details and the theory of data analysis are provided in the Supporting Information, S3.

ASSOCIATED CONTENT

Supporting Information

Detailed information on mass determination, supplementary methods, transient absorption spectroscopy measurements, quantum efficiency calculation, optical property analysis, and modeling the photoreduction response. This material is available free of charge via the Internet at http://pubs.acs.org.

AUTHOR INFORMATION

Corresponding Authors

*Tel: 1-(314) 935-5482. Fax: 1-(314) 935-5464. E-mail: pbiswas@wustl.edu.

*Tel: 1-(314) 935-3537. Fax: 1-(314) 935-4014. E-mail: parag.banerjee@wustl.edu.

Author Contributions

W.N.W. and F.W. contributed equally to this work. W.N.W., F.W., P.Ba., and P.Bi. designed the research and experiments. F.W. fabricated ZnO−CuO nanowires and conducted materials characterization. W.N.W. performed photocatalytic analysis. D.M.N. did transient absorption measurements. Y.M., H.S.I., and J.P. conducted PL measurements. W.N.W and P.Ba. wrote the paper. All authors contributed to the discussion.

Notes

The authors declare no competing financial interest.

ACKNOWLEDGMENTS

This work was supported by the Consortium for Clean Coal Utilization (CCCU) at Washington University in St. Louis (WUSTL). Partial support from the Nano Research Facility (NRF, a member of NSF-NNIN) is greatly acknowledged.

DOI: 10.1021/am508590j
ACS Appl. Mater. Interfaces 2015, 7, 5685−5692

Funding from McDonnell Academy Global Energy and Environment Partnership (MAGEEP) and the International Center for Advanced Renewable Energy & Sustainability (I-CARES) is acknowledged. Microscopy facilities were provided by the Institute of Materials Science and Engineering at WUSTL. ALD precursors were provided with generous support from SAFC Hitech®. AFM facilities from Professor Srikanth Singamaneni's lab are gratefully acknowledged. Time-resolved TA spectroscopy was performed in the ultrafast laser facility of Photosynthetic Antenna Research Center, an Energy Frontier Research Center funded by the U.S. DOE, Office of Basic Energy Sciences (Grant No. DE-SC 0001035).

REFERENCES

(1) Recent Monthly Average Mauna Loa CO_2. www.esrl.noaa.gov/gmd/ccgg/trends/index.html.
(2) Barnosky, A. D.; Hadly, E. A.; Bascompte, J.; Berlow, E. L.; Brown, J. H.; Fortelius, M.; Getz, W. M.; Harte, J.; Hastings, A.; Marquet, P. A.; Martinez, N. D.; Mooers, A.; Roopnarine, P.; Vermeij, G.; Williams, J. W.; Gillespie, R.; Kitzes, J.; Marshall, C.; Matzke, N.; Mindell, D. P.; Revilla, E.; Smith, A. B. Approaching a State Shift in Earth's Biosphere. *Nature* **2012**, *486* (7401), 52−58.
(3) Wang, W.; Wang, S. P.; Ma, X. B.; Gong, J. L. Recent Advances in Catalytic Hydrogenation of Carbon Dioxide. *Chem. Soc. Rev.* **2011**, *40* (7), 3703−3727.
(4) Inoue, T.; Fujishima, A.; Konishi, S.; Honda, K. Photoelectrocatalytic Reduction of Carbon Dioxide in Aquesous Suspensions of Semiconductor Powders. *Nature* **1979**, *277*, 637.
(5) Usubharatana, P.; McMartin, D.; Veawab, A.; Tontiwachwuthikul, P. Photocatalytic Process for CO_2 Emission Reduction from Industrial Flue Gas Streams. *Ind. Eng. Chem. Res.* **2006**, *45* (8), 2558−2568.
(6) Indrakanti, V. P.; Kubicki, J. D.; Schobert, H. H. Photoinduced Activation of CO_2 on Ti-based Heterogeneous Catalysts: Current State, Chemical Physics-based Insights and Outlook. *Energy Environ. Sci.* **2009**, *2* (7), 745−758.
(7) Roy, S. C.; Varghese, O. K.; Paulose, M.; Grimes, C. A. Toward Solar Fuels: Photocatalytic Conversion of Carbon Dioxide to Hydrocarbons. *ACS Nano* **2010**, *4* (3), 1259−1278.
(8) Dhakshinamoorthy, A.; Navalon, S.; Corma, A.; Garcia, H. Photocatalytic CO_2 Reduction by TiO_2 and Related Titanium Containing Solids. *Energy Environ. Sci.* **2012**, *5* (11), 9217−9233.
(9) Kondratenko, E. V.; Mul, G.; Baltrusaitis, J.; Larrazabal, G. O.; Perez-Ramirez, J. Status and Perspectives of CO_2 Conversion into Fuels and Chemicals by Catalytic, Photocatalytic and Electrocatalytic Processes. *Energy Environ. Sci.* **2013**, *6* (11), 3112−3135.
(10) Habisreutinger, S. N.; Schmidt-Mende, L.; Stolarczyk, J. K. Photocatalytic Reduction of CO_2 on TiO_2 and Other Semiconductors. *Angew. Chem., Int. Ed.* **2013**, *52* (29), 7372−7408.
(11) Fujishima, A.; Zhang, X. T.; Tryk, D. A. TiO_2 Photocatalysis and Related Surface Phenomena. *Surf. Sci. Rep.* **2008**, *63* (12), 515−582.
(12) Linsebigler, A. L.; Lu, G. Q.; Yates, J. T. Photocatalysis on TiO_2 Surfaces—Principles, Mechanisms, and Selected Results. *Chem. Rev.* **1995**, *95* (3), 735−758.
(13) Fujishima, A.; Honda, K. Electrochemical Photolysis of Water at a Semiconductor Electrode. *Nature* **1972**, *238* (5358), 37−38.
(14) Rajeshwar, K. Solar Energy Conversion and Environmental Rennediation Using Inorganic Semiconductor-Liquid Interfaces: The Road Traveled and the Way Forward. *J. Phys. Chem. Lett.* **2011**, *2* (11), 1301−1309.
(15) Kubacka, A.; Fernandez-Garcia, M.; Colon, G. Advanced Nanoarchitectures for Solar Photocatalytic Applications. *Chem. Rev.* **2012**, *112* (3), 1555−1614.
(16) Woolerton, T. W.; Sheard, S.; Reisner, E.; Pierce, E.; Ragsdale, S. W.; Armstrong, F. A. Efficient and Clean Photoreduction of CO_2 to CO by Enzyme-Modified TiO_2 Nanoparticles using Visible Light. *J. Am. Chem. Soc.* **2010**, *132* (7), 2132−2133.
(17) Tseng, I. H.; Chang, W. C.; Wu, J. C. S. Photoreduction of CO_2 using Sol−Gel Derived Titania and Titania-Supported Copper Catalysts. *Appl. Catal., B* **2002**, *37* (1), 37−48.
(18) Koci, K.; Mateju, K.; Obalova, L.; Krejcikova, S.; Lacny, Z.; Placha, D.; Capek, L.; Hospodkova, A.; Solcova, O. Effect of Silver Doping on the TiO_2 for Photocatalytic Reduction of CO_2. *Appl. Catal., B* **2010**, *96* (3−4), 239−244.
(19) Wang, W. N.; An, W. J.; Ramalingam, B.; Mukherjee, S.; Niedzwiedzki, D. M.; Gangopadhyay, S.; Biswas, P. Size and Structure Matter: Enhanced CO_2 Photoreduction Efficiency by Size-resolved Ultrafine Pt Nanoparticles on TiO_2 Single Crystals. *J. Am. Chem. Soc.* **2012**, *134* (27), 11276−11281.
(20) Ikeue, K.; Yamashita, H.; Anpo, M.; Takewaki, T. Photocatalytic Reduction of CO_2 with H_2O on Ti-β Zeolite Photocatalysts: Effect of the Hydrophobic and Hydrophilic Properties. *J. Phys. Chem. B* **2001**, *105* (35), 8350−8355.
(21) Lin, W. Y.; Han, H. X.; Frei, H. CO_2 Splitting by H_2O to CO and O_2 Under UV Light in TiMCM-41 Silicate Sieve. *J. Phys. Chem. B* **2004**, *108* (47), 18269−18273.
(22) Wang, W. N.; Park, J.; Biswas, P. Rapid Synthesis of Nanostructured Cu−TiO_2−SiO_2 Composites for CO_2 Photoreduction by Evaporation Driven Self-Assembly. *Catal. Sci. Technol.* **2011**, *1* (4), 593−600.
(23) Liu, L. J.; Zhao, C. Y.; Zhao, H. L.; Pitts, D.; Li, Y. Porous Microspheres of MgO-patched TiO_2 for CO_2 Photoreduction with H_2O Vapor: Temperature-Dependent Activity and Stability. *Chem. Commun.* **2013**, *49* (35), 3664−3666.
(24) Varghese, O. K.; Paulose, M.; LaTempa, T. J.; Grimes, C. A. High-Rate Solar Photocatalytic Conversion of CO_2 and Water Vapor to Hydrocarbon Fuels. *Nano Lett.* **2009**, *9* (2), 731−737.
(25) Zhou, H.; Guo, J. J.; Li, P.; Fan, T. X.; Zhang, D.; Ye, J. H. Leaf-Architectured 3D Hierarchical Artificial Photosynthetic System of Perovskite Titanates Towards CO_2 Photoreduction into Hydrocarbon Fuels. *Sci. Rep.* **2013**, *3*, 1667.
(26) Satoh, N.; Hasegawa, H.; Tsujii, K.; Kimura, K. Photoinduced Coagulation of Au Nanocolloids. *J. Phys. Chem.* **1994**, *98* (8), 2143−2147.
(27) Song, C. S. Global Challenges and Strategies for Control, Conversion, and Utilization of CO_2 for Sustainable Development Involving Energy, Catalysis, Adsorption, and Chemical Processing. *Catal. Today* **2006**, *115* (1−4), 2−32.
(28) Tahir, M.; Amin, N. S. Photocatalytic CO_2 Reduction and Kinetic Study Over In/TiO_2 Nanoparticles Supported Microchannel Monolith Photoreactor. *Appl. Catal., A* **2013**, *467*, 483−496.
(29) Wu, F.; Myung, Y.; Banerjee, P. Unravelling Transient Phases During Thermal Oxidation of Copper for Dense CuO Nanowire Growth. *CrystEngComm* **2014**, *16*, 3264−3267.
(30) Jiang, X. C.; Herricks, T.; Xia, Y. N. CuO Nanowires Can Be Synthesized by Heating Copper Substrates in Air. *Nano Lett.* **2002**, *2* (12), 1333−1338.
(31) Woll, C. The Chemistry and Physics of Zinc Oxide Surfaces. *Prog. Surf. Sci.* **2007**, *82* (2−3), 55−120.
(32) Zhao, J. H.; Han, E. J.; Liu, T. M.; Zeng, W. First-Principles Study on Electronic Properties of Low-Index ZnO Surfaces. *Asian J. Chem.* **2012**, *24* (7), 2903−2908.
(33) Vayssieres, L. Growth of Arrayed Nanorods and Nanowires of ZnO From Aqueous Solutions. *Adv. Mater.* **2003**, *15* (5), 464−466.
(34) Ohyama, M.; Kozuka, H.; Yoko, T. Sol−Gel Preparation of ZnO Films with Extremely Preferred Orientation Along (002) Plane from Zinc Acetate Solution. *Thin Solid Films* **1997**, *306* (1), 78−85.
(35) Bian, Z.; Tachikawa, T.; Zhang, P.; Fujitsuka, M.; Majima, T. A Nanocomposite Superstructure of Metal Oxides with Effective Charge Transfer Interfaces. *Nat. Commun.* **2013**, *5*, 3038.
(36) Wu, F.; Tian, L.; Kanjolia, R.; Singamaneni, S.; Bnerjee, P. Plasmonic Metal-to-Semiconductor Switching in Au Nanorod-ZnO Nanocomposite Films. *ACS Appl. Mater. Interfaces* **2013**, *5*, 7693−7697.
(37) Othonos, A.; Zervos, M. Ultrafast Hole Carrier Relaxation Dynamics in *p*-type CuO Nanowires. *Nanoscale Res. Lett.* **2011**, *6*, 1−5.

DOI: 10.1021/am508590j
ACS Appl. Mater. Interfaces 2015, 7, 5685−5692

(38) Panigrahy, B.; Aslam, M.; Misra, D. S.; Ghosh, M.; Bahadur, D. Defect-Related Emissions and Magnetization Properties of ZnO Nanorods. *Adv. Funct. Mater.* **2010**, *20* (7), 1161−1165.
(39) Zhu, Y. W.; Sow, C. H.; Yu, T.; Zhao, Q.; Li, P. H.; Shen, Z. X.; Yu, D. P.; Thong, J. T. L. Co-synthesis of ZnO−CuO Nanostructures by Directly Heating Brass in Air. *Adv. Funct. Mater.* **2006**, *16* (18), 2415−2422.
(40) Djurisic, A. B.; Leung, Y. H. Optical Properties of ZnO Nanostructures. *Small* **2006**, *2* (8−9), 944−961.
(41) Shalish, I.; Temkin, H.; Narayanamurti, V. Size-dependent Surface Luminescence in ZnO Nanowires. *Phys. Rev. B* **2004**, *69* (24), 245401.
(42) Lin, Y. J.; Tsai, C. L.; Lu, Y. M.; Liu, C. J. Optical and Electrical Properties of Undoped ZnO Films. *J. Appl. Phys.* **2006**, *99* (9), 093501.
(43) Dingle, R. Luminescent Transitions Associated with Divalent Copper Impurities and the Green Emission from Semiconducting Zinc Oxide. *Phys. Rev. Lett.* **1969**, *23* (11), 579−81.
(44) Ye, J. D.; Gu, S. L.; Zhu, S. M.; Chen, T.; Liu, W.; Qin, F.; Hu, L. Q.; Zhang, R.; Shi, Y.; Zheng, Y. D. Raman and Photoluminescence of ZnO Films Deposited on Si (111) using Low-pressure Metalorganic Chemical Vapor Deposition. *J. Vac. Sci. Technol., A* **2003**, *21* (4), 979−982.
(45) Chang, Y.-M.; Jian, S.-R.; Lee, H.-Y.; Lin, C.-M.; Juang, J.-Y. Enhanced Visible Photoluminescence from Ultrathin ZnO Films Grown on Si-nanowires by Atomic Layer Deposition. *Nanotechnology* **2010**, *21* (38), 385705.
(46) Tamaki, Y.; Furube, A.; Murai, M.; Hara, K.; Katoh, R.; Tachiya, M. Dynamics of Efficient Electron-hole Separation in TiO_2 Nanoparticles Revealed by Femtosecond Transient Absorption Spectroscopy under the Weak-Excitation Condition. *Phys. Chem. Chem. Phys.* **2007**, *9* (12), 1453−1460.
(47) Pankove, J. I. *Optical Processes in Semiconductors*. Dover Publication, Inc.: New York, 1975.
(48) Rothenberger, G.; Moser, J.; Gratzel, M.; Serpone, N.; Sharma, D. K. Charge Carrier Trapping and Recombination Dynamics in Small Semiconductor Particles. *J. Am. Chem. Soc.* **1985**, *107* (26), 8054−8059.
(49) Alam, M. A.; Green, M. L. Mathematical Description of Atomic Layer Deposition and Its Application to the Nucleation and Growth of HfO_2 Gate Dielectric Layers. *J. Appl. Phys.* **2003**, *94* (5), 3403−3413.
(50) Chang, J.; Ahmed, R.; Wang, H.; Liu, H.; Lo, R.; Wang, P.; Waclawik, E. R. ZnO Nanocones with High-Index {10$\bar{1}$1} Facets for Enhanced Energy Conversion Efficiency of Dye-Sensitized Solar Cells. *J. Phys. Chem. C* **2013**, *117* (27), 13836−13844.

DOI: 10.1021/am508590j
ACS Appl. Mater. Interfaces 2015, 7, 5685−5692